



Stochastic Scenarios for 21st Century Rainfall Seasonality, Daily Frequency, and Intensity in South Florida

Francesco Cioffi¹; Federico Rosario Conticello²; and Upmanu Lall³

Abstract: We demonstrate that a nonhomogeneous hidden Markov model (NHMM) can be useful for simulating future daily rainfall at 19 stations in South Florida. Using upper atmosphere circulation variables that are typically better represented than precipitation in general circulation models (GCMs), a NHMM conditioned on GCM circulation variables is shown to provide credible stochastic simulations of daily precipitation for future conditions. Seasonality changes as well as changes in seasonal extreme precipitation quantiles, total seasonal rainfall, and number of wet days are assessed. The Coupled Model Intercomparison Project phase 5 simulation of the coupled ocean-atmosphere Euro-Mediterranean Center on Climate Change Climate Model CMCC-CMS for 1948–2100 is used for the demonstration. Seasonality changes emerge naturally from the driving variables, and each season is not modeled separately. The future projections for CMCC-CMS indicate that South Florida may have drier conditions for most of the year. The number of wet days reduces, while extreme rainfall frequency increases. These findings are consistent with recent rainfall trends. A modest reduction in total rainfall in the February–May period and a slight increase in the September–October projected rainfall is noted. Changes in the expression of the North Atlantic subtropical high in the CMCC-CMS simulations appear to influence the new seasonality and patterns of rainfall. DOI: 10.1061/(ASCE)WR.1943-5452.0001250. © 2020 American Society of Civil Engineers.

Introduction

Climate change poses a number of problems for the management and restoration of Everglades National Park and for the multiple objectives for the management of the water infrastructure in South Florida. Changes due to anthropogenic global warming in rainfall seasonality, intermittence, and intensity, together with variations of temperature, sea level, and hurricane occurrence, may interact and determine the potential outcomes for surface and groundwater flows as well as other factors such as flooding, erosion, mangrove retreat, salinity, and ecological diversity (Orton et al. 2018; Merz et al. 2014; Cioffi 2008; Cioffi et al. 2017). The understanding of such phenomena could lead to the development of better tools for water management and water supply systems (e.g., Cioffi et al. 2015; Salas et al. 2012). Existing water simulation models use stochastic rainfall sequences indexed to existing rain gauges, and consequently, extending such simulations to future conditions is of pragmatic interest.

Obeysekera et al. (2011) provide a review and analysis of climate change projections for the region. In addition, many authors relate the interannual variability in regional precipitation to the dynamics of the El Niño–Southern Oscillation (ENSO) (Hanson and Maul 1991; Hagemeyer 2006; Schmidt et al. 2001; Beckage et al.

2003; Abteu and Trimble 2010; Kwon et al. 2006), Atlantic thermohaline circulation (ATC) (Gray et al. 1997; Landsea et al. 1996), North Atlantic Oscillation (NAO) (Walker and Bliss 1932), Arctic Oscillation (AO) (Thompson and Wallace 1998), Atlantic Multidecadal Oscillation (AMO) (Enfield et al. 2001; Curtis 2008; Miralles-Wilhelm et al. 2005; Mestas-Nuñez and Enfield 2003; Teegavarapu et al. 2013), and Pacific Decadal Oscillation (PDO) (Trenberth and Hurrell 1994). These phenomena modulate the atmospheric circulation and moisture transport mechanisms worldwide (Zhu and Newell 1998; Lavers and Villarini 2015; Conticello et al. 2018), thus influencing regional precipitation.

Hidden Markov models (HMM) and nonhomogeneous Markov models (NHMM) (see, e.g., Zucchini and Guttorp 1991; Hughes and Guttorp 1994; Hughes et al. 1999; Charles et al. 1999; Bellone et al. 2000; Charles et al. 2004; Robertson et al. 2004; Betrò et al. 2008; Cioffi et al. 2016, 2017; Robertson et al. 2003; Hughes et al. 1999; Charles et al. 1999; Hewitson and Crane 2006) have been used successfully to model the link between precipitation and atmospheric variables, considering the regimelike behavior of precipitation in many studies, including in South Florida. The general structure of this approach is illustrated in Fig. 1. Kwon et al. (2009) proposed a general methodology for the multilevel modeling of low- and high-frequency phenomena, with wavelet autoregressive models applied to paleoclimate proxies used to simulate decadal climate variability, as predictors for the seasonal NHMM. Khalil et al. (2010) used NHMMs to forecast multisite seasonal precipitation in Everglades National Park, South Florida, for the two major rainy seasons of May–June–July (MJJ) and August–September–October (ASO) directly using preseason ocean and atmosphere predictors.

In these past applications, the NHMM was set up separately for each fixed season identified a priori. Here, we were interested in 21st century projections of precipitation, and part of the anthropogenic change of interest includes inference as to potential changes in rainfall seasonality. The relevance of this issue has been highlighted by a number of authors for North America, including Mallakpour and Villarini (2017) and Jiang et al. (2016), and for Florida by Gitau (2016), Wang et al. (2013), and Nungesser et al. (2015).

¹Professor, Dept. of Civil, Constructional and Environmental Engineering, Univ. of Rome “La Sapienza”, Rome 00184, Italy (corresponding author). ORCID: <https://orcid.org/0000-0002-5841-8405>. Email: francesco.cioffi@uniroma1.it

²Postdoctoral, Dept. of Civil, Constructional and Environmental Engineering, Univ. of Rome “La Sapienza”, Rome 00184, Italy. ORCID: <https://orcid.org/0000-0003-0614-0656>

³Professor, Dept. of Earth and Environmental Engineering, Columbia Univ. of New York, New York 10027. ORCID: <https://orcid.org/0000-0003-0529-8128>

Note. This manuscript was submitted on January 16, 2019; approved on February 10, 2020; published online on May 23, 2020. Discussion period open until October 23, 2020; separate discussions must be submitted for individual papers. This paper is part of the *Journal of Water Resources Planning and Management*, © ASCE, ISSN 0733-9496.

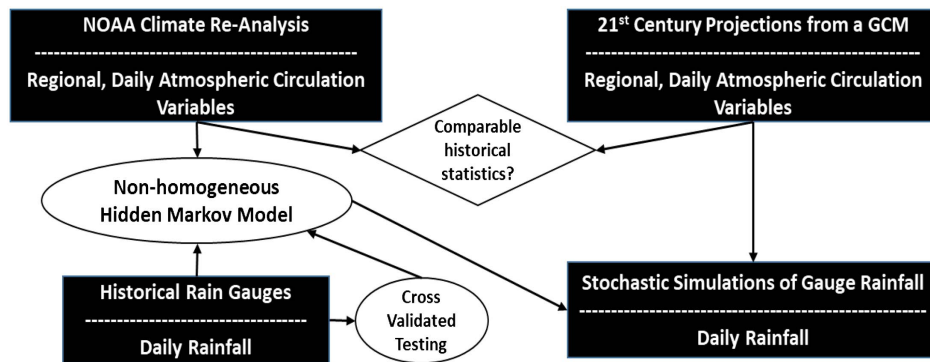


Fig. 1. General structure of the NHMM application. The stochastic process of the underlying daily rainfall across all the rain gauges in the region is considered to be influenced by unobserved weather regimes which conform to a Markovian process that is learned from the rainfall data. The probability of observing each of these regimes on a given day is also conditioned on atmospheric circulation variables that are available from reanalysis or from a future GCM projection. The correspondence of the statistics between the reanalysis and the historical GCM data over the same period is used to assess the suitability of the GCM for projection. Split sample testing of the NHMM in the historical period is used to assess whether trends in the rainfall statistics in the historical record are adequately reproduced using the atmospheric circulation variables.

Despite these notable contributions, how future changes in atmospheric circulation and related moisture transport drive potential changes in rainfall seasonality for Florida—locally depending on the complex interaction between the seasonal changes of Bermuda high strength and position (Li et al. 2011; Wang et al. 2010, 2013) and larger scale climate phenomenon such as ENSO—is still not clear. Consequently, in the NHMM developed in the current work, we explored whether dynamical variables related to the atmospheric circulation and moisture content could effectively inform changes in the seasonality of precipitation as well as in other key statistics of daily precipitation in South Florida, using a candidate scenario for the Coupled Model Intercomparison Project phase 5 (CMIP5) model.

Other approaches to map general circulation model (GCM) precipitation to rain gauge scales exist. These include bias correction methods, e.g., bias correction spatial disaggregation (BCSD) (Wood et al. 2004; Maurer et al. 2007), localized constructed analogs (LOCA) (Pierce et al. 2014), or multivariate adaptive constructed analogs (MACA) (Abatzoglou and Brown 2012). However, such methods are not seen as appropriate by some investigators (Ehret et al. 2012) because they do not readily provide a physical justification or address feedbacks. We do not review these methods here, because our interest was in being able to generate transient stochastic simulations that could better inform hydrologic scenarios for the region, and we were interested in potential insights into the physical mechanisms of change. Dynamic downscaling using regional climate models that use boundary conditions from GCMs would help provide physical insights, but would require considerably more computation to produce stochastic scenarios for water management applications. Hence, that approach was also not considered.

“Climate Context and Data” section provides an overview of the data used for the application to 19 stations in South Florida where a 65-year record (1948–2012) of rainfall was available. The NHMM methodology is described next in “Methods” section, followed by a presentation of the model fitting in “NHMM for South Florida” section. The predicted future rainfall patterns under a global warming scenario (RCP8.5), using predictors from the Euro-Mediterranean Center on Climate Change Climate Model (CMCC-CMS) simulations from 1948–2100, are then presented in “NHMM” section. We only consider this extreme scenario and a single GCM because our focus is on an exploration of whether the approach sketched in Fig. 1 can provide credible results for changes

in seasonality and rainfall statistics. Providing future scenarios for rainfall change in Florida considering multiple scenarios and models was not our goal. The application to other scenarios can be mechanically done, and an approach that would optimally combine simulations across multiple GCMs was considered beyond the scope of this paper. Applications to other GCMs could of course be mechanically done. A discussion of the results concludes the paper.

Climate Context and Data

The greater portion of Florida belongs to a wet subtropical climate. South Florida has a 5-month wet season that extends from late spring into the fall and a dry season of roughly 7 months that extends from late fall through spring. Superimposed on the main annual pattern is a short dry period within the summer, and in some years, brief periods of heavy rains occur in the middle of winter. Two phenomena are primarily responsible for the wet season rains: tropical storms, including hurricanes, and thunderstorms related to convection induced by thermal breeze winds. Winter rains are primarily associated with the passage of cold fronts, which sweep down into South Florida in late fall, winter, and early spring. Spring weather in South Florida is highly variable from year to year and depends on the position and size of the Bermuda High, which can hamper convective cloud development (Obeysekera et al. 1999).

In this study, we use a 65-year record (1948–2012) of daily rainfall amounts at 19 stations, whose locations are shown in Fig. 2 (for more details see also Fig. S1 and Table S1). The data were obtained from the KNMI Climate Explorer database.

Atmospheric Fields Selected for the NHMM

For the NHMM, the following daily atmospheric fields, collected both from reanalysis data and GCM runs, were considered as predictors: temperature (T) at 1,000 hPa, geopotential height (GPH) at 1,000 hPa, meridional winds (MW) and zonal winds (ZW) at 850 hPa, and zonal winds on the latitude of 27° N (ZW27N) from 10 to 1,000 hPa. The National Center for Environmental Prediction/National Center for Atmospheric Research (NCEP/NCAR) reanalysis fields (Kalnay et al. 1996) were downloaded from the website of the IRI/LDEO Climate Data Library (n.d.).

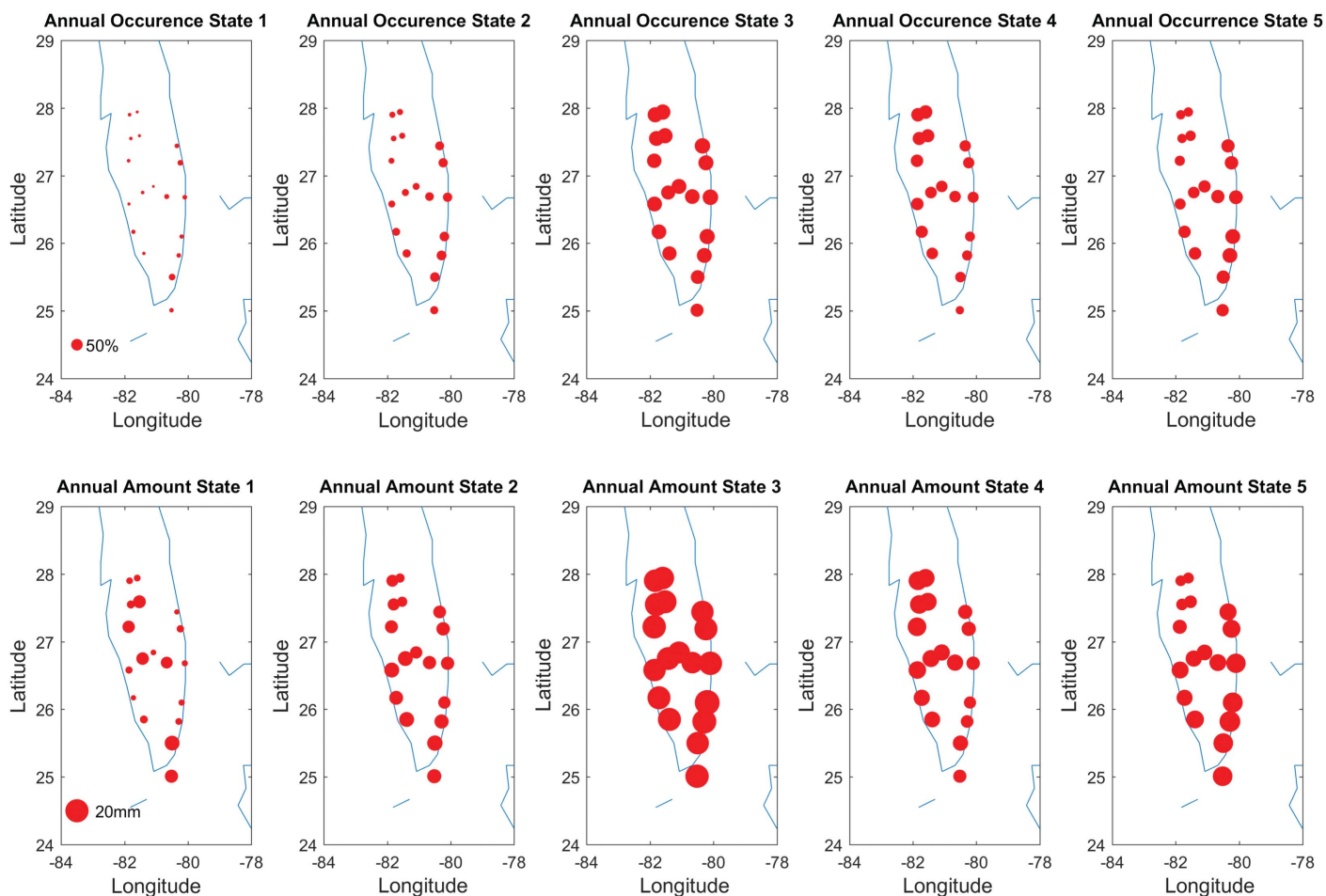


Fig. 2. Occurrence and mean amounts of daily rainfall for each of the five hidden states identified by HMM (annual period from 1948 to 2012 for 19 stations in Florida region).

The 21st century projections of rainfall patterns in South Florida were carried out using daily atmospheric fields from GCMs belonging to CMIP5 (Karl et al. 2009). Initially, two potential candidate GCMs were selected based on a literature review, namely, the CanEMS2 (Chylek et al. 2011) and the CMCC-CMS. For each of the NHMM predictors, we compared the basic statistics (seasonal mean, variance, skew, variance, and serial correlation) and the spatial pattern for each of the leading principal components (PCs) from the two candidate GCMs for each atmospheric field with the corresponding PCs from the NCEP/NCAR reanalysis. The period of 1948–2012 was used for these comparisons. The CMCC-CMS was selected based on this comparison. It couples the following models: ECHAM5 for atmosphere (Roeckner et al. 2006), OPA8.2 and the Louvain-La-Neuve sea-ice model (LIM) for ocean and sea ice (Madec et al. 1998), with OASIS3 as the coupler (Valcke et al. 2006, 2012). We understand that we could do a similar comparison for each GCM belonging to CMIP5, and subsequently do a weighted combination of GCMs based on their reliability in reproducing historical atmospheric circulation patterns for the region. However, this was not pursued in this work, because our primary focus was on exploring whether or not the NHMM is credible for reproducing changes in the seasonality and the key statistics of rainfall for changing conditions for the region. The combination of GCMs or the evaluation of their relative performance for the purpose could certainly be pursued given the success of this demonstration.

The reanalysis data from 1948 to 2012 and the CMCC-CMS data for 1948–2100 were downloaded. The fields of atmospheric variables were selected over the domain bounded by 10N–60N and 120W–0W. This region covers the likely large-scale controls on the rainfall pattern in South Florida.

For the CMCC-CMS future integration we considered only the Representative Concentration Pathways (RCP) 8.5 scenario for CMIP5. This is the most severe global warming scenario among those simulated (Hayhoe et al. 2017), because this would bracket potential changes across the other scenarios.

Methods

The HMM and NHMM models as presented by Kirshner (2005), Khalil et al. (2010), and Robertson et al. (2004) were adapted for the applications pursued in this paper. These models are outlined below for completeness, and the reader is referred to the earlier papers for details.

HMM

The HMM described in Khalil et al. (2010), Kirshner (2005), and Robertson et al. (2004) is based on the work of Hughes and Guttorg (1994).

Let $\mathbf{R}_t = (R_t^1, R_t^2, \dots, R_t^M)$ be a vector of rainfall amounts for a network of M stations on day t , and let $\mathbf{R}_{1:T}$ denote a time sequence of such vectors. This sequence of observed rainfall measurements is assumed to be generated by a Markov chain of hidden (unobserved) weather states \mathbf{S}_t , where \mathbf{S}_t takes values from 1 to K . Under a first-order Markov assumption, the joint distribution over the hidden state sequence can be factored as

$$p(\mathbf{S}_1, \mathbf{S}_2, \dots, \mathbf{S}_T) = p(\mathbf{S}_1) \prod_{t=2}^T p(\mathbf{S}_t | \mathbf{S}_{t-1}) \quad (1)$$

where $p(\mathbf{S}_t | \mathbf{S}_{t-1})$ is modeled as a $K \times K$ state transition probabilities matrix and $p(\mathbf{S}_1)$ is a set of initial state probabilities.

The rainfall \mathbf{R}_t on day t is assumed to depend only on the hidden state on day t . Thus

$$p(\mathbf{R}_{1:T}, \mathbf{S}_{1:T}) = p(\mathbf{S}_1) \prod_{t=2}^T p(\mathbf{S}_t | \mathbf{S}_{t-1}) \prod_{t=1}^T p(\mathbf{R}_t | \mathbf{S}_t) \quad (2)$$

It is further assumed that the M station components of the vector of rainfall amounts at time t are conditionally independent of each other given the hidden state \mathbf{S}_t , i.e., spatial dependence is captured implicitly via the hidden state variable

$$p(\mathbf{R}_t | \mathbf{S}_t) = p(\mathbf{S}_t) \prod_{m=1}^M p(R_t^m | \mathbf{S}_t) \quad (3)$$

The probability models for individual stations, $p(\mathbf{R}_t | \mathbf{S}_t)$, are specified using a delta function, corresponding to zero precipitation, and a mixture gamma to model the non-zero amount distribution, i.e.,

$$p(\mathbf{r}_t | \mathbf{S}_t = i) = \prod_{m=1}^M a_{im} \left\{ \begin{array}{ll} p_{im0} & r_t^m = 0 \\ \sum_{c=1}^{C-1} p_{imc} \frac{\phi_{imc}^{\omega_{imc}} (r_t^m)^{\omega_{imc}-1} e^{-\phi_{imc} r_t^m}}{\Gamma(\omega_{imc})} & r_t^m > 0 \end{array} \right\} \quad (4)$$

where p_{im0} = probability of no precipitation for state i for station m , in the conditionally independent gamma mixture model for rainfall amounts; p_{im1} = complementary probability of rainfall; and ϕ_{imc} and ω_{imc} = parameters of the gamma distribution for each component c in the mixture model. For our application a single gamma distribution worked best in terms of the usual performance measures for model fitting, e.g., the Bayesian information criterion (BIC).

The parameters of the model are estimated from the observed rainfall amount data using the expectation maximization (EM) algorithm. The rainfall amounts are incorporated directly into the formulation of the HMM, similar to the approach of Bellone et al. (2000). Details of the EM estimation algorithm were presented by Robertson et al. (2004), who considered only binary precipitation occurrence instead of rainfall amounts and occurrence for each latent state, as is done here. The EM equations required to handle estimation of the parameters for the state-dependent amount models are as described in Kirshner (2005).

In order to identify the most probable sequence of states associated to observations, the Viterbi algorithm is used (Viterbi 1967), whose details are provided in Bellone et al. (2000) and Kirshner (2005).

NHMM

NHMMs relate the hidden states identified from the local rainfall data to regional atmospheric circulation patterns. The assumption is that latent weather states act as a link between the large atmospheric scale and the regional rainfall. (Hughes et al. 1999). Let $\mathbf{X}_t = (X_t^1, X_t^2, \dots, X_t^p)$ be a sequence of p exogenous atmospheric variables at time t . Following Kirshner (2005), the NHMM is defined through

$$p(\mathbf{R}_t | \mathbf{S}_t^1, \mathbf{R}_{t-1}, \mathbf{X}_t^1) = p(\mathbf{R}_t | \mathbf{S}_t) p(\mathbf{S}_t | \mathbf{S}_{t-1}, \mathbf{X}_t) \quad (5)$$

where \mathbf{X}_t^1 = sequence of atmospheric data from time 1 to t (i.e., the length of sequence); and \mathbf{S}_t^1 = hidden state vector up to time t .

As a result, the statistics of daily rainfall from the NHMM process vary over time based on the time variation of the inputs \mathbf{X}_t . These hidden state transitions are modeled by multinomial logistic regression depending on \mathbf{X}_t :

$$p(\mathbf{S}_t = i | \mathbf{S}_t = j, \mathbf{X}_t = \mathbf{x}) = \frac{e^{(\alpha_{ji} + \beta_j^T \mathbf{x})}}{\sum_{k=1}^K e^{(\alpha_{jk} + \beta_k^T \mathbf{x})}} \quad (6)$$

where α_{ji} and β_j^T = parameters for the multinomial regression.

Applying the EM algorithm (Baum et al. 1970; Robertson et al. 2003), the maximum likelihood estimate of the set of parameters for the NHMM-based application is calculated. Calibration and simulation phases were performed by the NHMM source code written by Kirshner, and the BIC is used for the selection of the predictors to retain.

NHMM for South Florida

Identification of Hidden States and Spatial Dependence Structure

Seasonality can change over time under anthropogenic forcing. Thus, one needs to actually inform these changes by the dynamics of the circulation system that change in the GCM simulations. We explore whether an identification of hidden states from the precipitation dynamics and the associated atmospheric circulation variables helps define the changes in the seasonality of precipitation in the region, simply by specifying future atmospheric circulation. With this in mind, we do not assume a priori delimitation of seasons, but consider the full year of data. Two possible approaches were considered for the spatial dependence of rainfall stations. These are the conditional independence model (HMM-CI) and the Chow-Liu tree model (HMM-CL) (see Kirshner et al. 2004). The first assumes that once the hidden state is known, the rainfall across the stations is independent. If this assumption is not tenable, then the HMM-CL provides a parsimonious approach to identify the multivariate dependence structure. Our initial analysis of spatial correlation across the 19 sites in South Florida, by season, indicated only weak spatial correlations. Nevertheless, we used the BIC criteria as well as cross-validation to explore the best number of hidden states and the corresponding spatial dependence model. Based on these analyses, the HMM-CI representation was selected, with five hidden states deemed as sufficient to recognize the seasonality of rainfall as well as the dependence on the atmospheric circulation variables.

Fig. 2 shows for each state and for each of the 19 stations the annual occurrence probability (top) and the corresponding average rainfall amount (bottom) obtained by applying HMM-CI. Fig. 3 shows the annual daily frequency of the hidden states, with dashed

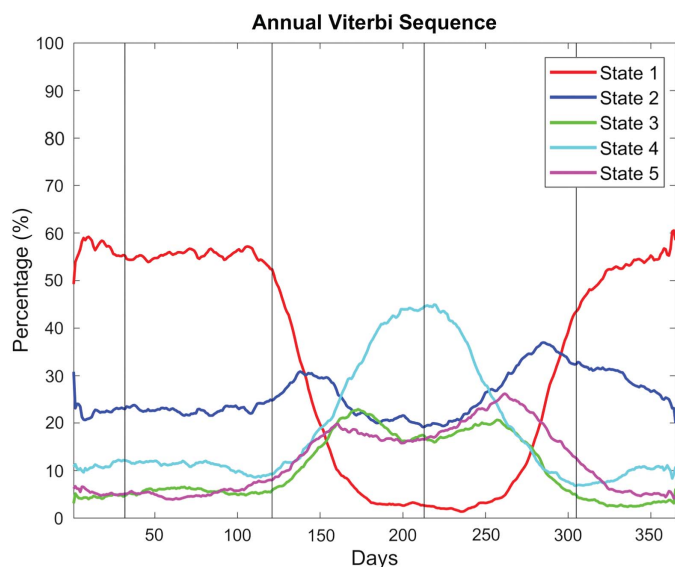


Fig. 3. Seasonality of the daily frequency of the hidden states (averaged over 1948–2012).

lines delimiting the hydrological seasons [November–December–January (NDJ), February–March–April (FMA), May–June–July (MJJ), and August–September–October (ASO)] of Florida. In the following the characteristics of each of the such hidden states are presented.

State 1 corresponds to a very dry condition that is nearly homogeneous for all the stations. It is dominant during the winter and early spring, from November to April. It almost completely disappears from June to August.

State 2 is not quite as dry. Its occurrence probabilities are generally very low for all the stations, but occurrence is higher for the stations closer to the coast, and rainfall amounts are higher than for State 1. This state persists through the entire year but with two maxima at the beginning of May and at the end of October. From November to April the occurrence probability is almost constant and greater than about 20%. The minimum occurrence of State 2 appears in summer from June to September.

State 3 corresponds to very wet conditions. Both high daily precipitation amounts and high rainfall occurrence probability (more than 50%) are homogeneous for all the stations. This state is absent in winter, with an increase in the occurrence probability (up to 20%) at the end of May and at the end of August.

State 4 can be defined as a wet spatially nonhomogeneous condition, because the rainfall occurrence probability is around 50% for most of the stations, but the coastal stations on the west side of the peninsula have a higher daily precipitation amount and occurrence probability. The state occurrence probability is maximum (>50%) between July and August. It dominates the July–August–September season. The occurrence probability declines to less than 10% in the winter.

State 5 represents a very wet but spatially nonhomogeneous condition, where the rainfall occurrence probability and daily amount are higher in the stations of the East Coast. Its temporal occurrence probability is very similar to that of State 3.

The hidden state classification identified suggests that the hidden states correspond to the different precipitation regimes that have a distinct seasonality. Consequently, exploring large-scale atmospheric predictors that can inform these mechanisms and the frequency of occurrence of these hidden states has promise for the

detection of projected changes in the intensity and seasonality of the rainfall statistics at the 19 stations analyzed.

NHMM Atmospheric Predictor Set Selection and Characteristics of Hidden States

For candidate atmospheric predictors for NHMM, we selected a domain of large-scale atmospheric circulation fields bounded by latitude from 10° N to 60° N and longitude from 120° E to 0°. The domain covers the Atlantic Ocean, a part of the Eastern Pacific Ocean, and is large enough to represent potential regional drivers of the local climate of the Florida region, including the strength and position of the Bermuda High in the Atlantic and of ENSO or PDO interactions with the Atlantic atmospheric circulation (Schmidt et al. 2001; Enfield et al. 2001).

Candidate atmospheric predictors identified from the 1948–2012 NCEP/NCAR reanalysis data were: temperature (T) at 1,000 hPa, geopotential height (GPH) at 1,000 hPa, meridional winds (MW) and zonal winds (ZW) at 850 hPa, and zonal winds at the latitude of 27° N (ZW27N) from 10 to 1,000 hPa for the 17 layers in the vertical. The temperature implicitly carries the information associated with warming and with the associated atmospheric moisture-holding capacity, and the pressure and wind variables included inform the circulation dynamics associated with the moisture transport into the region and the potential precipitation dynamics. Specifically, (a) the persistence and daily anomalies of GPH and T fields at 1,000 hPa may be linked to the seasonality of circulation in the region, including convection events and the passage of fronts; and (b) potential cyclonic and anticyclonic flows can be identified by the zonal and meridional wind fields at 850 hPa and (c) by the zonal wind fields on the vertical plane (27° N and 120° E to 0°) from 10 to 1,000 hPa, which collectively represent the three-dimensional structure of the circulation.

For each candidate predictor, composite fields for each hidden state were obtained by averaging anomalies of predictor variable fields across all days that are associated with that hidden state based on the Viterbi sequence identified by HMM. The physical consistency (based on the expected thermodynamics of the meteorological processes affecting moisture transport and precipitation) between the composite fields and the expected rainfall characteristics associated with each hidden state was assessed to select the final subset of predictors.

The GPH fields are shown in Fig. 4. The mean field (top left) represents a semipermanent, subtropical area of high pressure in the North Atlantic Ocean off the East Coast of North America that migrates east and west with varying central pressure. When it is displaced westward, during the northern hemispheric summer and fall, the center is located in the western North Atlantic, near Bermuda. In the winter and early spring, it is primarily centered near the Azores in the eastern part of the North Atlantic. State 1 occurs primarily in the winter, and the associated GPH shows the corresponding shift, which is consistent with expectation. The anomaly field of State 2 (middle left plot) is weak and does not significantly alter the mean annual field. States 3 and 5 show very similar GPH patterns, with a dipole oriented in the northwest direction whose high and low pressure centers are opposite to those of State 1. Although, the high pressure center of States 3 and 5 has the same intensity and location, the low pressure center of State 3 is closer to Florida and significantly more intense than that of State 5. In State 4 the dipole moves west and rotates counterclockwise with respect to those for States 3 and 5. The intensity of high and low pressure centers is similar to those of State 5, but less intense than for State 3.

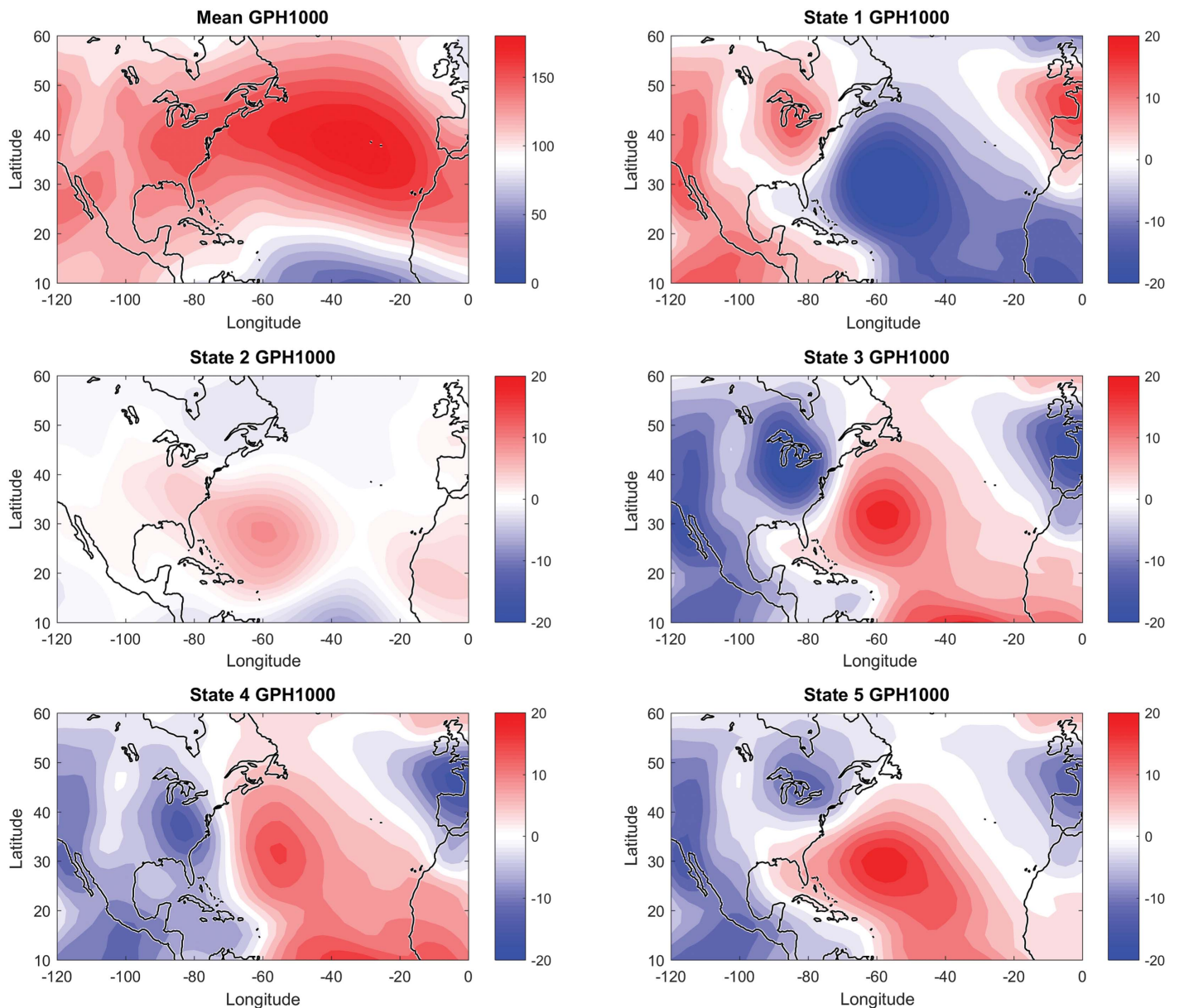


Fig. 4. GPH at 1,000 hPa; Reanalysis data: IRI Library -NOAA-NCAR. (Data from Kalnay et al. 1996.)

The temperature anomaly fields (Fig. S2) are similar for States 3–5 and exhibit a nearly opposite anomaly pattern to State 1, as one may expect from the summer/winter predominant expression of these states. They are weak for State 2.

Zonal and meridional winds anomaly fields at 850 hPa of each state are analyzed also (Fig. S3). States 1 and 2, associated with winter dry conditions, are characterized by wind anomalies with anticyclonic flow tendencies toward the Florida peninsula from the northwest and northeast, whereas the remaining states show the dominance of cyclonic anomalies from the south approaching the Florida peninsula at different angles from the east or west, consistent with the rainfall patterns in Fig. 2 and the GPH patterns in Fig. 4.

Vertical patterns of zonal wind at 27° N of latitude (corresponding to the mean latitude of the Florida peninsula) for each state are analyzed (Fig. S4). State 1 (dry winter) and States 3–5 (wet summer) are distinguished by the reversion of the sign of zonal wind anomalies, positive for State 1 and negative for the other ones.

As before, State 2 has low anomaly values that are positive (negative) on the west (east) side.

Dimension reduction by principal component analysis (PCA) was performed for each of the selected atmospheric variable fields. By considering the leading PCs of these regional atmospheric fields in the model, we expect to capture the dominant characteristics of the circulation, its seasonal and interannual variation, and the resulting effects on regional precipitation.

NHMM Calibration and Validation for Different Predictor Sets

A number of statistical rainfall indices (shown in Table 1), rainfall amount, number of wet days, and the 50%, 90%, 95%, and 99% daily rainfall are compared for 1948–1982 and 1983–2012, both for the observations at the 19 sites and for the simulations of the model for the two periods, with the model parameters estimated using only

Table 1. Number of stations out of 19 with a higher value of the statistic in 1983–2012 compared to the 1948–1982 period, illustrating macrolevel trends in rainfall and its extremes. Bold face indicates an entry significantly different from what would be expected by chance at the 5% level using a binomial test. Only in MJJ is a significant decrease indicated for rain amount and the 99th percentile of daily rainfall

Season	Rain amount	Wet days (#)	Median rain	90th percentile rain	95th percentile rain	99th percentile rain
NDJ	19	12	8	13	11	18
FMA	15	11	11	13	13	8
MJJ	5	6	9	11	9	4
ASO	15	7	12	16	15	16

the first period. The indices are calculated for each of the four seasons, defined usually as FMA, MJJ, ASO, and NDJ, even though the model fitting is done for the full year and is not constrained by these season definitions. We see from Table 1 that in terms of total rainfall, and the extremes of rainfall, these two periods are significantly different from each other at the 5% significance level for most seasons. Given that these periods are shown to be statistically different in terms of the rainfall statistics, a demonstration that the model fit on the first period can predict the statistics for this later period would be a good proof of concept.

A cross-validated framework was used to assess the performance of the proposed NHMM. The model was fit for different candidate predictor sets on the 1948–2002 data. The NHMM fit in the prior period was then applied using the atmospheric circulation data for the period 2003–2012. The resulting spatiotemporal statistics covering seasonality as well as rainfall quantiles and wet-day frequency were then compared with the observed rainfall statistics, specifically to assess whether the directional changes in these statistics relative to the prior period were informed by the candidate NHMM.

Different combinations of leading PCs from each candidate field were used to explore the performance of the model. We chose the number of PCs that explains at least 80% of the variance. This led to five GPH PCs, two T PCs, five MW PCs, five ZW PCs, and two MW27N PCs.

After fitting each candidate model, 100 simulations are generated for 2003–2012 using the reanalysis PCs from that period as predictors for each candidate NHMM model, and the statistics of these are then compared to those of the observed 2003–2012 data. The squared errors between the mean simulated statistic for each season and the observed statistic for the season for each of the indices considered are provided for each candidate model in Table S1.

The model NHMM + GTW fit well on both number of wet days and seasonal rainfall (see, Figs. S5 and S6). This model also does well in reproducing seasonality and the distribution of the 90th and 99th percentiles of daily rainfall across the 19 stations for each season (see, Fig. S7). Consequently, we conclude that the NHMM as implemented with reanalysis-based predictors is capable of a credible out-of-sample prediction for a period whose rainfall statistics were noted to be different from the prior period of the climate record. The application with the CMIP5 GCM is considered next.

Potential of NHMM to Project Changes in South Florida Rainfall for the 21st Century

The leading PCs of atmospheric predictors extracted from the CMCC-CMS simulations were used as input to NHMM. We found that both leading PCs and spatial patterns of each field from the

reanalysis and the GCM are comparable, but the PC temporal variances differ. To make the PCs from CMCC-CMS statistically consistent with those for the NCEP/NCAR reanalysis, we followed the following procedure.

The variance-corrected predictor for the 21st century PCs from CMCC-CMS is defined as

$$PC_{jt}^{M21c} = PC_{jt}^{M21} \times s(PC_{jt}^{O20}) / s(PC_{jt}^{M20})$$

where the standard deviation is $s(\cdot)$; PC_{jt}^{M20} = historical time series of the j th predictor from the GCM; PC_{jt}^{O20} = corresponding time series for the reanalysis observations; and PC_{jt}^{M21} and PC_{jt}^{M21c} refer to the GCM time series for the 21st century and its corrected version, respectively. PC_{jt}^{M21c} is then used for the 21st century NHMM simulations.

The approach was verified for simulating rainfall with the NHMM using, as inputs, predictors from NCEP/NCAR reanalysis and a CMCC-CMS control run for the common period of record. The statistics of the two series generated by the simulation are similar for rainfall percentile and for the wet seasons, MJJ and ASO, with some modest differences for the NDJ and FMA seasons (Fig. S8). The statistics for the simulations generated without the variance correction were not comparable.

For the RCP8.5 climate change scenario, simulations were carried out using the CMCC-CMS-derived variance-corrected PCs from 1948 to 2100. In Figs. 5 and 6, the 21st century bidecadal simulation results for 2020–2040, 2040–2060, and 2080–2100 are compared with the control run simulation from 1986 to 2006. We note a progressive negative trend of number of wet days and seasonal rainfall amount in all the seasons, except for ASO, where we observe a modest increase in both rainfall amount and wet days. Correspondingly, the number of dry days increases in all the seasons, with the exception of ASO, where no significant changes occur.

An estimate of the change in rainfall statistics is made by taking the difference between the mean of the index in a future 20-year period (2080–2100) and the mean of the index for 1986–2006 (Figs. S9–S12). For all seasons except ASO, we note that the principal trends are a decrease in the number of wet days and total rainfall amount and an increase in the 99th percentile of daily rainfall across the stations. Interestingly, the median daily wet-day rainfall (not shown) does not undergo a significant change. For ASO, the number of wet days increases, especially along the East Coast, and the results for the other indices are mixed, with some indication of a modest increase in total rainfall.

An illustration of the changes in the large-scale circulation from 1986–2006 to 2080–2100 is provided for selected months to understand possible factors that lead to the changes in the rainfall indices. From Fig. 7(a) bottom (showing the difference in the temperature fields for 2080–2100 in respect to 1986–2006), note the increased warming at the poles in March, the associated weaker equator-to-pole temperature gradient, and the slightly weaker land-ocean temperature contrast between the normally warmer Atlantic Ocean and the North American continent that warms slightly more. The corresponding shift in the GPH field [see top plot of Fig. 7(a)] shows a prominent displacement of the North Atlantic subtropical high to the southwest and an adjustment of the polar circulation such that there is lower pressure in the area that experiences the most polar warming at the northeastern edge of North America, higher pressures over Iceland, and lower pressures in the Azores and mid-continent North America, reflecting that a meridional moisture transport is likely shifted west of Florida, resulting in a reduction in the number of wet days in this period. However, the warmer

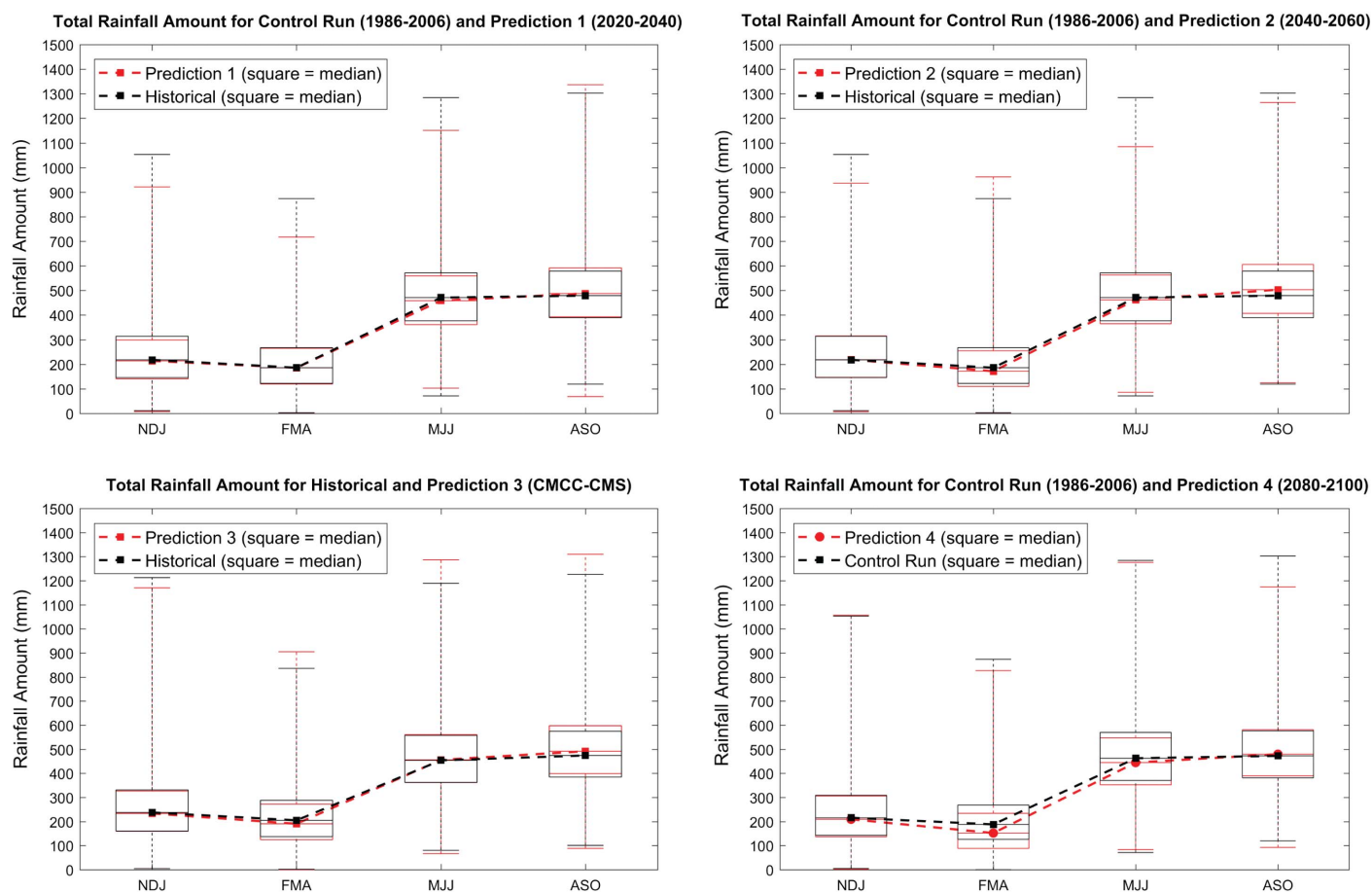


Fig. 5. Comparison between the total seasonal rainfall amounts for the period 1986–2006 and for the different 20-year periods (2020–2040, 2040–2060, 2060–2080, and 2080–2100).

temperatures likely lead to higher moisture in the atmosphere, which, in conjunction with the frontal systems active in this time period, lead to increased extreme precipitation. These changes are consistent with what one expects from the potential changes in the equator-to-pole temperature gradient and the land-ocean temperature contrast (Jain et al. 1999; Karamperidou et al. 2012). In June [Fig. 7(b)] the warming is considerably smaller than in March, and while there is still a weakening of the equator-to-pole temperature gradient, the intensification of the warming over the center of North America and the Euro-African land mass is much more noticeable. This translates to lower pressures over the Western Mediterranean and the polar regions and a southwestward shift of the North Atlantic subtropical high pressure to the Florida region, which has the effect of steering storms away from the region. This phenomenon is noted also by Li et al. (2011, 2012) and Gamble et al. (2008).

Summary and Discussion

In this paper, we focused on exploring what can be learned from the projections suggested by a single GCM as to the regional mechanisms and directions of change in the seasonality and statistics of daily rainfall. We identified atmospheric circulation fields that influence the regional precipitation and used them to build a physically informed stochastic simulation model for daily rainfall in the region. The model builds on past related work in the region, and the

key innovation is the use of the atmospheric circulation variables from the GCM to inform the dynamics of both the seasonality and rainfall at the same time. The success in this demonstration suggests that a more flexible approach for stochastic downscaling from GCMs is feasible and could be applied for different scenarios and GCMs.

Scientific consensus on climate change suggests that global warming could induce an increase in extreme rainfall but a reduction of the frequency of subtropical rainfall. By the Clausius-Clapeyron equation, higher temperature leads to higher water vapor concentration in the atmospheric column. This suggests that extreme precipitation events may increase. Mechanisms of atmospheric convergence and divergence and changes in the large-scale atmospheric circulation fields, due to persistent modifications in the surface boundary conditions, are also important. The analyses presented indicate an increase in the magnitude of the 90th and 99th percentile of the daily rainfall, while the median daily rainfall is largely unchanged in the Florida projections through the end of the 21st century. We note a continuation of the observed trend for a decrease in the number of wet days and in the seasonal rainfall amount for all seasons except for ASO, when there is a modest increase. A seasonally variable change in the surface temperature gradients and in the North Atlantic subtropical high is seen to alter the rainfall attributes in Florida by changing the steering winds. This is consistent with the dynamics reported in the literature and is seen in the CMIP5 scenario for the model we selected for downscaling. There is a potential reduction of groundwater recharge due

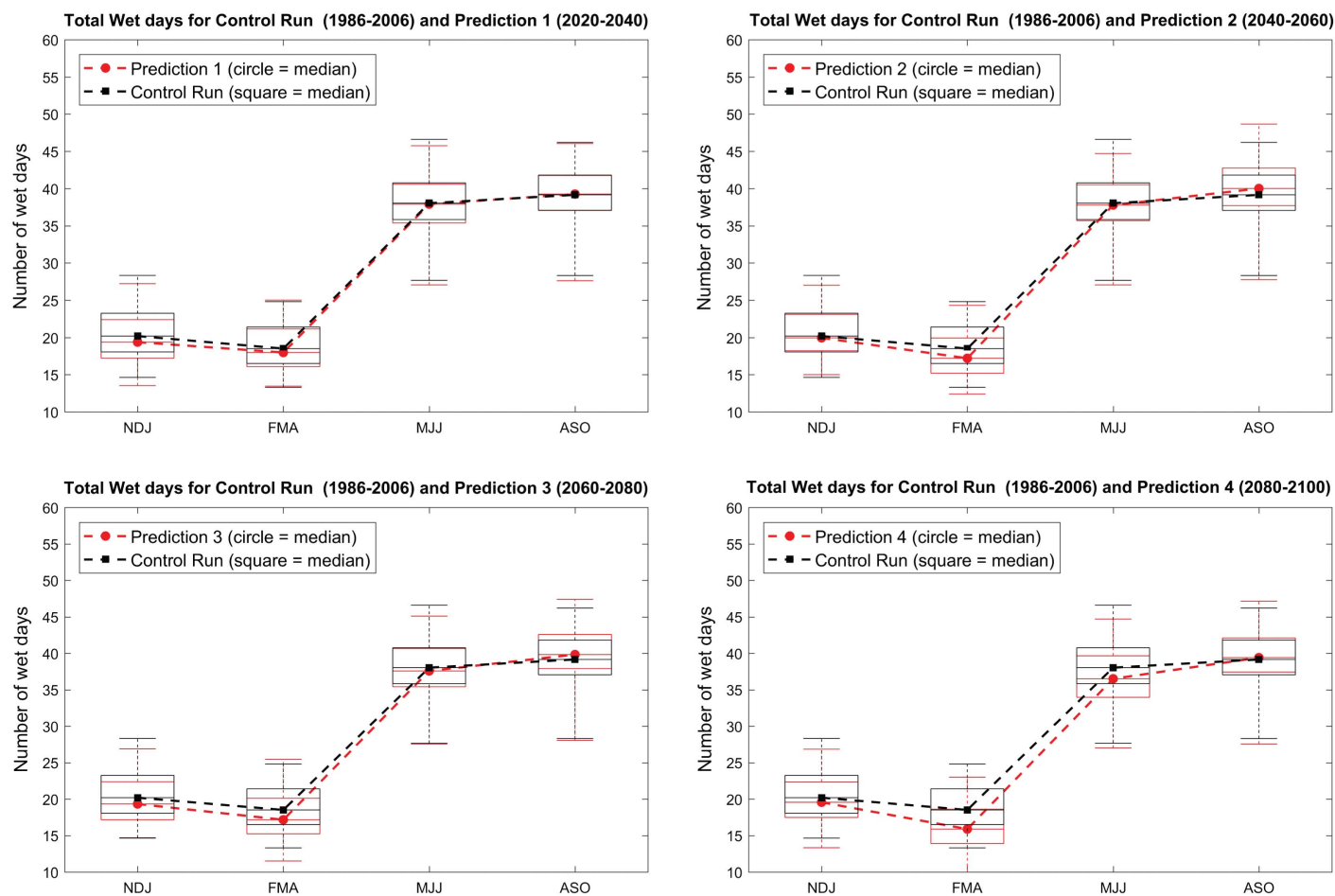


Fig. 6. Comparison between the number of wet days for the period 1986–2006 and for the different 20-year periods (2020–2040, 2040–2060, 2060–2080, and 2080–2100).

to the longer dry spells and lower overall rainfall. Given this observation, without pursuing a hydrologic model that uses the daily precipitation sequences (and other climate variables), it is not clear whether the increase in the upper percentiles of rainfall would always translate into higher flood risk, as may be expected from the observed trend in these statistics.

We found that the spatial patterns of the large-scale atmospheric circulation fields were, in general, reasonable in the retrospective simulations of the selected model, including the seasonality and the temporal pattern of the annual cycle. However, the amplitudes of the leading patterns were not often consistent with those from the reanalysis model that was used to fit the NHMM. Correcting the variance of these leading circulation modes for each predictor field resulted in an improvement in the quality of the rainfall simulations downscaled from the retrospective run of the GCM. This is an important diagnostic. As a matter of principle, we are not in favor of a bias correction approach to the historical statistics of the GCM simulations to extrapolate to the future scenarios. It is not clear whether, in the absence of an understanding of why the biases exist between a particular GCM's retrospective run and the corresponding reanalysis run, one can make useful extrapolations into the future. For the application here, our correction is effectively equivalent to using a standardized (i.e., normalized to a mean of 0 and standard deviation of 1) time series for the reanalysis and for the GCM. However, the variance mismatch in the historical period calls for an investigation of the factors that lead to the differences

between the atmospheric circulation fields in the reanalysis model versus the GCM.

The identification of predictors and how to structure the model are major challenges in any statistical downscaling exercise, and while there is a formal way to pose and estimate the model, choosing a set of predictors remains an art to quite an extent. In that context, the work presented here can be considered one useful case study out of many such examples. Finally, multiple model combinations and different RCP scenarios should be taken into account if the results of the study are to be presented to stakeholders as part of a discussion of the range of uncertainty that is realistic. An extension to multiple models and scenarios is then mechanically possible but does not add to the demonstration we explored for the CMCC-CMS and RCP8.5. Other GCMs will most likely give different detailed results, given that the model and parameter uncertainties have been demonstrated to be significant globally and regionally. Consequently, if future projections for Florida precipitation were of interest, the use of only one model and one scenario is a limitation.

In addition to the significant uncertainties across GCMs with regard to precipitation, it is likely that South Florida will experience significant changes in vegetation and water/land percentages as sea levels rise and the changing climate leads to vegetative changes and also changes in human settlement. At some point such local structural changes may be more important than the changes in precipitation. Such factors are currently not accounted for in climate model simulations or in local response modeling. The integrated

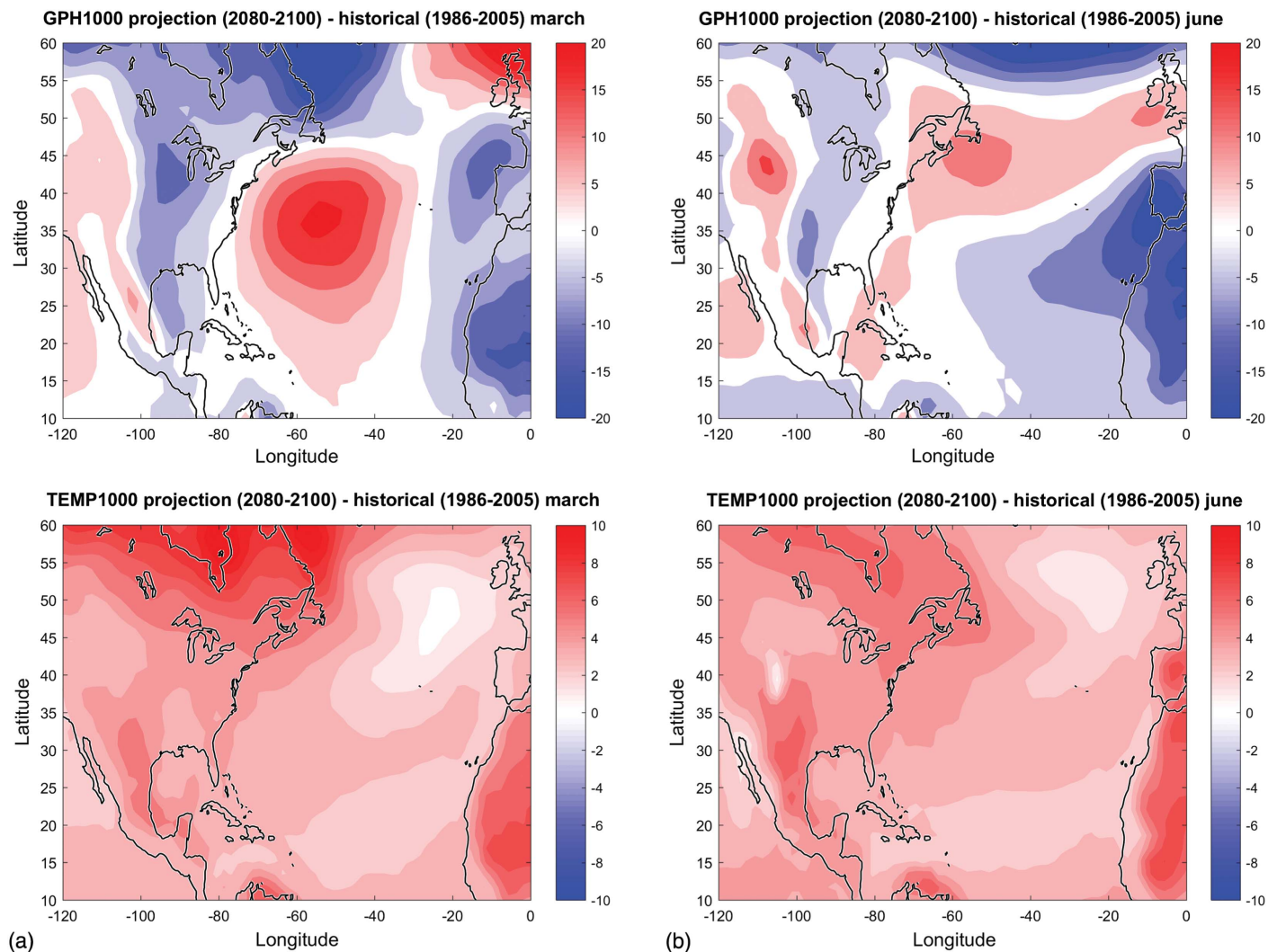


Fig. 7. Change in the mean GPH and temperature fields for (a) March; and (b) June from 1986–2006 to 2080–2100.

modeling of these processes far out in the future poses a major challenge.

Data Availability Statement

In this study, we use daily rainfall amounts obtained from the KNMI Climate Explorer database (<https://climexp.knmi.nl>). Daily fields of atmospheric variables are obtained from both reanalysis data and GCM runs. The NCEP/NCAR reanalysis fields (Kalnay et al. 1996) were downloaded from the website of the International Research Institute for Climate and Society (www.iri.columbia.edu). Data from GCM runs were downloaded from the Earth System Grid Federation–Lawrence Livermore National Laboratory node (<https://esgf-node.llnl.gov/projects/esgf-llnl/>). The multivariate nonhomogeneous hidden Markov model toolbox used to perform simulation is available at <http://www.sergeykirshner.com>.

Acknowledgments

The research reported here was supported by the US National Park Service under Contract No. H5284-08-0003. The support of the H2CU program for the research agreement between Columbia

University and the University of Roma, La Sapienza is gratefully acknowledged.

Supplemental Materials

Figs. S1–S12 and Tables S1 and S2 are available online at www.ascelibrary.org.

References

- Abatzoglou, J. T., and T. J. Brown. 2012. "A comparison of statistical downscaling methods suited for wildfire applications." *Int. J. Climatol.* 32 (5): 772–780. <https://doi.org/10.1002/joc.2312>.
- Abtey, W., and P. Trimble. 2010. "El Niño–Southern Oscillation link to South Florida hydrology and water management applications." *Water Resour. Manage.* 24 (15): 4255–4271. <https://doi.org/10.1007/s11269-010-9656-2>.
- Baum, L. E., T. Petrie, G. Soules, and N. Weiss. 1970. "A maximization technique occurring in the statistical analysis of probabilistic functions of Markov chains." *Ann. Math. Stat.* 41 (1): 164–171. <https://doi.org/10.1214/aoms/1177697196>.
- Beckage, B., W. J. Platt, M. G. Slocum, and B. Panko. 2003. "Influence of the El Niño Southern Oscillation on fire regimes in the Florida Everglades." *Ecol. Ecol. Soc. Am.* 84 (12): 3124–3130.

- Bellone, E., J. P. Hughes, and P. Guttorp. 2000. "A hidden Markov model for downscaling synoptic atmospheric patterns to precipitation amounts." *Clim. Res.* 15 (1): 1–12. <https://doi.org/10.3354/cr015001>.
- Bettrò, B., A. Bodini, and Q. A. Cossu. 2008. "Using a hidden Markov model to analyse extreme rainfall events in Central-East Sardinia." *Environmetrics* 19 (7): 702–713.
- Charles, S. P., B. C. Bates, and J. P. Hughes. 1999. "A spatiotemporal model for downscaling precipitation occurrence and amounts." *J. Geophys. Res. Atmos.* 104 (D24): 31657–31669. <https://doi.org/10.1029/1999JD900119>.
- Charles, S. P., B. C. Bates, I. N. Smith, and J. P. Hughes. 2004. "Statistical downscaling of daily precipitation from observed and modelled atmospheric fields." *Hydrol. Processes* 18 (8): 1373–1394. <https://doi.org/10.1002/hyp.1418>.
- Chylek, P., J. Li, M. K. Dubey, M. Wang, and G. Lesins. 2011. "Observed and model simulated 20th century Arctic temperature variability: Canadian earth system model CanESM2." *Atmos. Chem. Phys. Discuss.* 11 (8): 22893–22907. <https://doi.org/10.5194/acpd-11-22893-2011>.
- Cioffi, F. 2008. "Dynamic behaviour of lagoon ecosystems." *Il Nuovo cimento della Società italiana di fisica. C* 31 (3): 281.
- Cioffi, F., F. Conticello, and U. Lall. 2016. "Projecting changes in Tanzania rainfall for the 21st century." *Int. J. Climatol.* 36 (13): 4297–4314. <https://doi.org/10.1002/joc.4632>.
- Cioffi, F., F. Conticello, U. Lall, L. Marotta, and V. Telesca. 2017. "Large scale climate and rainfall seasonality in a Mediterranean area: Insights from a non-homogeneous Markov model applied to the Agro-Pontino plain." *Hydrol. Processes* 31 (3): 668–686. <https://doi.org/10.1002/hyp.11061>.
- Cioffi, F., U. Lall, E. Rus, and C. K. B. Krishnamurthy. 2015. "Space-time structure of extreme precipitation in Europe over the last century." *Int. J. Climatol.* 35 (8): 1749–1760. <https://doi.org/10.1002/joc.4116>.
- Conticello, F., F. Cioffi, B. Merz, and U. Lall. 2018. "An event synchronization method to link heavy rainfall events and large-scale atmospheric circulation features." *Int. J. Climatol.* 38 (3): 1421–1437. <https://doi.org/10.1002/joc.5255>.
- Curtis, S. 2008. "The Atlantic multidecadal oscillation and extreme daily precipitation over the US and Mexico during the hurricane season." *Clim. Dyn.* 30 (4): 343–351. <https://doi.org/10.1007/s00382-007-0295-0>.
- Ehret, U., E. Zehe, V. Wulfmeyer, K. Warrach-Sagi, and J. Liebert. 2012. "Hydrology and earth system sciences HESS opinions 'Should we apply bias correction to global and regional climate model data?'" *Hydrol. Earth Syst. Sci.* 16 (9): 3391–3404. <https://doi.org/10.5194/hess-16-3391-2012>.
- Enfield, D. B., A. M. Mestas-Núñez, and P. J. Trimble. 2001. "The Atlantic multidecadal oscillation and its relation to rainfall and river flows in the continental U.S." *Geophys. Res. Lett.* 28 (10): 2077–2080. <https://doi.org/10.1029/2000GL012745>.
- Gamble, D. W., D. B. Parnell, and S. Curtis. 2008. "Spatial variability of the Caribbean mid-summer drought and relation to north Atlantic high circulation." *Int. J. Climatol.* 28 (3): 343–350. <https://doi.org/10.1002/joc.1600>.
- Gitau, M. 2016. "Long-term seasonality of rainfall in the southwest Florida Gulf coastal zone." *Climate Research* 69 (2): 93–105. <https://doi.org/10.3354/cr01399>.
- Gray, W. M., J. D. Sheaffer, and C. W. Landsea. 1997. "Climate trends associated with multidecadal variability of atlantic hurricane activity." In *Hurricanes: Climate and socioeconomic impacts*, edited by H. F. Diaz, and R. Pulwarty, 15–53. Berlin: Springer.
- Hagemeyer, B. C. 2006. "ENSO, PNA and NAO scenarios for extreme storminess, rainfall and temperature variability during the Florida dry season." In *Proc., 18th Conf. on Climate Variability and Change*. Boston: American Meteorological Society.
- Hanson, K., and G. Maul. 1991. "Florida precipitation and the Pacific El Niño, 1985-1989." *Florida Sci. FLSCAQ* 54 (3/4): 161–168.
- Hayhoe, K., J. Edmonds, R. E. Kopp, A. N. LeGrande, B. M. Sanderson, M. F. Wehner, and D. J. Wuebbles. 2017. "Climate models, scenarios, and projections." In Vol. I of *Climate science special report: Fourth national climate assessment*, edited by D. J. Wuebbles, D. W. Fahey, K. A. Hibbard, B. C. Stewart, and T. K. Maycock. Washington, DC: Fourth National Climate Assessment.
- Hewitson, B. C., and R. G. Crane. 2006. "Consensus between GCM climate change projections with empirical downscaling: Precipitation downscaling over South Africa." *Int. J. Climatol.* 26 (10): 1315–1337. <https://doi.org/10.1002/joc.1314>.
- Hughes, J. P., and P. Guttorp. 1994. "A class of stochastic models for relating synoptic atmospheric patterns to regional hydrologic phenomena." *Water Resour. Res.* 30 (5): 1535–1546. <https://doi.org/10.1029/93WR02983>.
- Hughes, J. P., P. Guttorp, and S. P. Charles. 1999. "A non-homogeneous hidden Markov model for precipitation occurrence." *J. R. Stat. Soc. Ser. C: Appl. Stat.* 48 (1): 15–30. <https://doi.org/10.1111/1467-9876.00136>.
- IRI/LDEO Climate Data Library (International Research Institute/Lamont-Doherty Earth Observatory Climate Data Library). n.d.. "Climate Data Library." Accessed May 17, 2020. <https://iridl.ldeo.columbia.edu/>.
- Jain, S., U. Lall, and M. E. Mann. 1999. "Seasonality and interannual variations of northern hemisphere temperature: Equator-to-pole gradient and ocean-land contrast." *J. Clim.* 12 (4): 1086–1100. [https://doi.org/10.1175/1520-0442\(1999\)012<1086:SAIVON>2.0.CO;2](https://doi.org/10.1175/1520-0442(1999)012<1086:SAIVON>2.0.CO;2).
- Jiang, M., B. Felzer, and D. Sahagian. 2016. "Predictability of precipitation over the conterminous US based on the CMIP5 multi-model ensemble." *Sci. Rep.* 6. <https://doi.org/10.1038/srep29962>.
- Kalnay, E., et al. 1996. "The NCEP/NCAR 40-year reanalysis project." *Bull. Am. Meteorol. Soc.* 77 (3): 437–471. [https://doi.org/10.1175/1520-0477\(1996\)077<0437:TNYRP>2.0.CO;2](https://doi.org/10.1175/1520-0477(1996)077<0437:TNYRP>2.0.CO;2).
- Karamperidou, C., F. Cioffi, and U. Lall. 2012. "Surface temperature gradients as diagnostic indicators of midlatitude circulation dynamics." *J. Clim.* 25 (12): 4154–4171. <https://doi.org/10.1175/JCLI-D-11-00067.1>.
- Karl, T. R., J. M. Melillo, T. C. Peterson, and S. J. Hassol. 2009. *A state of knowledge report from the U.S. global change research program*. In *Global Climate Change Impacts in the United States: A State of Knowledge Report from the US Global Climate Change Research Program*, edited by K. R. Thomas, M. M. Jerry, C. P. Thomas, and J. H. Susan. New York: Cambridge University Press.
- Khalil, A. F., H.-H. Kwon, U. Lall, and Y. H. Kaheil. 2010. "Predictive downscaling based on non-homogeneous hidden Markov models." *Hydrol. Sci. J.* 55 (3): 333–350. <https://doi.org/10.1080/02626661003780342>.
- Kirshner, S. 2005. "Modeling of multivariate time series using hidden Markov models." Ph.D thesis, Dept. of Information and Computer Sciences, Univ. of California.
- Kirshner, S., P. Smyth, and A. W. Robertson. 2004. "Conditional chowliu tree structures for modeling discrete-valued vector time series." In *Proc., 20th Conf. on Uncertainty in Artificial Intelligence*, 317–324. Edinburgh, Scotland: AUAI Press.
- Kwon, H. H., U. Lall, Y. II Moon, A. F. Khalil, and H. Ahn. 2006. "Episodic interannual climate oscillations and their influence on seasonal rainfall in the Everglades National Park." *Water Resour. Res.* 42 (11): 1–14. <https://doi.org/10.1029/2006WR005017>.
- Kwon, H. H., U. Lall, and J. Obeysekera. 2009. "Simulation of daily rainfall scenarios with interannual and multidecadal climate cycles for South Florida." *Stochastic Environ. Res. Risk Assess.* 23 (7): 879–896. <https://doi.org/10.1007/s00477-008-0270-2>.
- Landsea, C. W., N. Nicholls, W. M. Gray, and L. A. Avila. 1996. "Downward trends in the frequency of intense Atlantic hurricanes during the past five decades." *Geophys. Res. Lett.* 23 (13): 1697–1700. <https://doi.org/10.1029/96GL01029>.
- Lavers, D. A., and G. Villarini. 2015. "The contribution of atmospheric rivers to precipitation in Europe and the United States." *J. Hydrol.* 522 (Mar): 382–390. <https://doi.org/10.1016/j.jhydrol.2014.12.010>.
- Li, L., W. Li, and Y. Kushnir. 2012. "Variation of the North Atlantic subtropical high western ridge and its implication to Southeastern US summer precipitation." *Clim. Dyn.* 39 (6): 1401–1412. <https://doi.org/10.1007/s00382-011-1214-y>.
- Li, W., L. Li, R. Fu, Y. Deng, and H. Wang. 2011. "Changes to the north Atlantic subtropical high and its role in the intensification of summer

- rainfall variability in the southeastern United States." *J. Clim.* 24 (5): 1499–1506. <https://doi.org/10.1175/2010JCLI3829.1>.
- Maded, G., P. Delecluse, M. Imbard, and C. Lévy. 1998. *OPA 8.1 ocean general circulation model reference manual*. Paris: Institut Pierre Simon Laplace des Sciences de l'environnement Global.
- Mallakpour, I., and G. Villarini. 2017. "Analysis of changes in the magnitude, frequency, and seasonality of heavy precipitation over the contiguous USA." *Theor. Appl. Climatol.* 130 (1–2): 345–363. <https://doi.org/10.1007/s00704-016-1881-z>.
- Maurer, E. P., L. Brekke, T. Pruitt, and P. B. Duffy. 2007. "Fine-resolution climate projections enhance regional climate change impact studies." *Eos, Trans. Am. Geophys. Union* 88 (47): 504. <https://doi.org/10.1029/2007EO470006>.
- Merz, B., et al. 2014. "Floods and climate: Emerging perspectives for flood risk assessment and management." *Nat. Hazard Earth Syst. Sci.* 14 (7): 1921–1942. <https://doi.org/10.5194/nhess-14-1921-2014>.
- Mestas-Núñez, A. M., and D. B. Enfield. 2003. *Investigation of intra-seasonal to multi-decadal variability in South Florida rainfall*. Miami: Atlantic Oceanographic and Meteorological Laboratory.
- Miralles-Wilhelm, F., P. J. Trimble, G. P. Podestà, and D. Letson. 2005. "Climate-based estimation of hydrologic inflow into Lake Okeechobee, Florida." *J. Water Resour. Plann. Manage.* 131 (5): 394–401. [https://doi.org/10.1061/\(ASCE\)0733-9496\(2005\)131:5\(394\)](https://doi.org/10.1061/(ASCE)0733-9496(2005)131:5(394)).
- Nungesser, M., C. Saunders, C. Coronado-Molina, J. Obeysekera, J. Johnson, C. McVoy, and B. Benschoter. 2015. "Potential effects of climate change on Florida's Everglades." *Environ. Manage.* 55 (4): 824–835. <https://doi.org/10.1007/s00267-014-0417-5>.
- Obeysekera, J., J. Browder, L. Hornung, and M. Harwell. 1999. "The natural South Florida system. I: Climate, geology, and hydrology." *Urban Ecosyst.* 3 (3/4): 223–244. <https://doi.org/10.1023/A:1009552500448>.
- Obeysekera, J., M. Irizarry, J. Park, J. Barnes, and T. Dessalegne. 2011. "Climate change and its implications for water resources management in South Florida." *Stochastic Environ. Res. Risk Assess.* 25 (4): 495–516. <https://doi.org/10.1007/s00477-010-0418-8>.
- Orton, P. M., F. R. Conticello, F. Cioffi, T. M. Hall, N. Georgas, U. Lall, A. F. Blumberg, and K. MacManus. 2018. "Flood hazard assessment from storm tides, rain and sea level rise for a tidal river estuary." In *Natural hazards*, 1–29. New York: Springer.
- Pierce, D. W., D. R. Cayan, and B. L. Thrasher. 2014. "Statistical downscaling using localized constructed analogs (LOCA)." *J. Hydrometeorol.* 15 (6): 2558–2585.
- Robertson, A. W., S. Kirshner, and P. Smyth. 2003. *Hidden Markov models for modeling daily rainfall occurrence over Brazil*. Technical Rep. No. UCI-ICS 03-27. Irvine, CA: Information and Computer Science Univ. of California.
- Robertson, A. W., S. Kirshner, and P. Smyth. 2004. "Downscaling of daily rainfall occurrence over Northeast Brazil using a hidden Markov model." *J. Clim.* 17 (22): 4407–4424. <https://doi.org/10.1175/JCLI-3216.1>.
- Roeckner, E., R. Brokopf, M. Esch, M. A. Giorgetta, S. Hagemann, L. Kornbluh, E. Manzini, U. Schlese, and U. Schulzweida. 2006. "Sensitivity of simulated climate to horizontal and vertical resolution in the ECHAM5 atmosphere model." *J. Clim.* 19 (16): 3771–3791. <https://doi.org/10.1175/JCLI3824.1>.
- Salas, J. D., B. Rajagopalan, L. Saito, and C. Brown. 2012. "Special section on climate change and water resources: Climate nonstationarity and water resources management." *J. Water Resour. Plann. Manage.* 385–388. [https://doi.org/10.1061/\(ASCE\)WR.1943-5452.0000279](https://doi.org/10.1061/(ASCE)WR.1943-5452.0000279).
- Schmidt, N., E. K. Lipp, J. B. Rose, and M. E. Luther. 2001. "ENSO influences on seasonal rainfall and river discharge in Florida." *J. Clim.* 14 (4): 615–628. [https://doi.org/10.1175/1520-0442\(2001\)014<0615:EOSRA>2.0.CO;2](https://doi.org/10.1175/1520-0442(2001)014<0615:EOSRA>2.0.CO;2).
- Teegavarapu, R., A. Goly, and J. Obeysekera. 2013. "Influences of Atlantic multidecadal oscillation phases on spatial and temporal variability of regional precipitation extremes." *J. Hydrol.* 495 (Jul): 74–93. <https://doi.org/10.1016/j.jhydrol.2013.05.003>.
- Thompson, D. W. J., and J. M. Wallace. 1998. "The Arctic oscillation signature in the wintertime geopotential height and temperature fields." *Geophys. Res. Lett.* 25 (9): 1297–1300. <https://doi.org/10.1029/98GL00950>.
- Trenberth, K. E., and J. W. Hurrell. 1994. "Decadal atmosphere-ocean variations in the Pacific." *Clim. Dyn.* 9 (6): 303–319. <https://doi.org/10.1007/BF00204745>.
- Valcke, S. 2012. "The OASIS3 coupler: A European climate modelling community software." *Geosci. Model Dev. Discuss.* 5: 2139–2178. <https://doi.org/10.5194/gmdd-5-2139-2012>.
- Valcke, S., E. Guilyardi, and C. Larsson. 2006. "PRISM and ENES: A European approach to Earth system modelling." *Concurrency Comput. Pract. Exp.* 18 (2): 247–262. <https://doi.org/10.1002/cpe.915>.
- Viterbi, A. J. 1967. "Error bounds for convolutional codes and an asymptotically optimum decoding algorithm." *IEEE Trans. Inf. Theory* 13 (2): 260–269. <https://doi.org/10.1109/TIT.1967.1054010>.
- Walker, G., and E. Bliss. 1932. "World weather V." *Memories R. Meteorol. Soc.* 4 (36): 53–84.
- Wang, D., S. C. Hagen, and K. Alizad. 2013. "Climate change impact and uncertainty analysis of extreme rainfall events in the Apalachicola River basin, Florida." *J. Hydrol.* 480 (Feb): 125–135. <https://doi.org/10.1016/j.jhydrol.2012.12.015>.
- Wang, H., R. Fu, A. Kumar, and W. Li. 2010. "Intensification of summer rainfall variability in the southeastern United States during recent decades." *J. Hydrometeorol.* 11 (4): 1007–1018. <https://doi.org/10.1175/2010JHM1229.1>.
- Wood, A. W., L. R. Leung, V. Sridhar, and D. P. Lettenmaier. 2004. "Hydrologic implications of dynamical and statistical approaches to downscaling climate model outputs." *Clim. Change* 62 (1–3): 189–216. <https://doi.org/10.1023/B:CLIM.0000013685.99609.9e>.
- Zhu, Y., and R. E. Newell. 1998. "A proposed algorithm for moisture fluxes from atmospheric rivers." *Mon. Weather Rev.* 126 (3): 725–735. [https://doi.org/10.1175/1520-0493\(1998\)126<0725:APAFMF>2.0.CO;2](https://doi.org/10.1175/1520-0493(1998)126<0725:APAFMF>2.0.CO;2).
- Zucchini, W., and P. Guttorp. 1991. "A hidden Markov model for space-time precipitation." *Water Resour. Res.* 27 (8): 1917–1923. <https://doi.org/10.1029/91WR01403>.